Fine Chemical Engineering
http://ojs.wiserpub.com/index.php/FCE/

Research Article

Effect of Biomass-Based Catalyst in Walnut Shell/Polypropylene to BTX

Yanan Guo, Xin Pan, Qingjiao Zhu, Jingjing Ma, Qingjie Guo*

State Key Laboratory of High-efficiency Utilization of Coal and Green Chemical Engineering, Ningxia University, Yinchuan, China
E-mail: qingjie_guo@163.com

Received: 27 July 2021; **Revised:** 22 October 2021; **Accepted:** 9 November 2021

Abstract: Four biomass-based catalyst carriers with different pore structures were prepared by using a carbonization-activation method, followed by employment in the copyrolysis of Walnut Shell/Polypropylene (WNS/PP) to produce Benzene, Toluene and Xylene (BTX). Ten cycles were performed in each copyrolysis test in a bench-scaled tube furnace to determine the suitable pore size of the catalyst and excellent cycling performance for BTX production. In addition, Zn, Ni, and Ce were loaded with the selected catalyst carriers to synthesize the most suitable biomass-based catalyst. Results showed that the pore size and active center of the catalyst were the key factors affecting the WNS/PP catalytic copyrolysis. Biomass-based carrier with a pore size in the range of 0.55-1.2 nm was the most suitable to produce BTX in the optimal 10 cycle performance; it realized a relative BTX content of 9-20 area%, and a BTX mass yield of 23-67 mg/(g_{raw}) in the liquid-phase products from the WNS/PP copyrolysis. A catalyst loaded with 10 wt% Zn possessed the best catalytic effect with a relative BTX content of 39.49 area% , and a BTX yield of 111.13 mg/(g_{raw}).

***Keywords*:** walnut shell, polypropylene, catalyst, pore size, BTX

1. Introduction

Environmental pollution and energy scarcity resulting from the rapid consumption of fossil fuels are becoming increasingly serious.[1-4] In recent years, biomass has become favored by researchers due to its abundant resources, wide range of existence, and green and renewable characteristics.[5-7] The bio-oil obtained from the single pyrolysis of biomass has disadvantages such as high oxygen content, high acidity, low calorific value, high corrosiveness, and low usage rate, which adversely affect the effective usage.[8] Therefore, many researchers have improved the quality of oil through biomass or catalytic pyrolysis and achieved remarkable results.

Researchers have found that the effective hydrogen to carbon ratio ($H:C_{eff}$) is an essential factor in improving the quality of bio-oil. Biomass contains less hydrogen, and the $H:C_{eff}$ value is less than 0.3, so the quality of bio-oil is poor.[9] Waste plastics are rich in hydrogen, and can generate liquid, solid and gas products during pyrolysis.[10-12] So in a biomass pyrolysis process, adding hydrogen-rich materials can improve the $H:C_{eff}$ value of biomass to improve the quality of bio-oil. Ozsin et al.,[13] Sajdak et al.,[14] Johansson et al.,[15] Dewangan et al.,[16] Burra et al.,[17] and Hu et al.[18] studied the different biomasses and various hydrogen-rich materials, and their results showed that the addition of hydrogen-rich materials, such as polymers and waste plastics, during the biomass pyrolysis process has a positive synergistic effect

DOI: https://doi.org/10.37256/fce.3120221057

on the biomass pyrolysis. In addition, the moisture content and acidity are reduced and its yield increases, which can effectively improve the quality of oil. As a result, the copyrolysis of biomass and hydrogen-rich materials can availably enhance the $H:C_{eff}$ value and produce excellent quality bio-oil.

Plastic products are polymers with a high $H:C_{eff}$ value and are cheap and available, which is an ideal source of hydrogen feedstock. China's urban plastic production is expected to reach 250 million tons by 2025.[19] In the biomass pyrolysis process, waste plastics with high $H:C_{eff}$ values can be used as cheap hydrogen donors, which can promote the composition distribution of pyrolysis products and enhance the selectivity of aromatics in bio-oil as well as properly address environmental problems caused by waste plastics.[20,21]

Adding catalysts and hydrogen-rich materials in the copyrolysis process of biomass can further increase the yield of aromatics in liquid oil to solve the problems of high oxygen content, low heat value, and high acid content,[22] which is an effective technique to produce high-value liquid oil.[23,24] The frequently used catalysts are zeolite molecular sieves HZSM-5, HBate, MCM-41, HY, modified molecular sieves, and metal oxides. Qi et al.,[25] Hyung et al.,[26] Lin et al.,[27] and Zhao et al.[28] studied the catalytic of biomass and hydrogen-rich materials over microporous zeolites, and their results have shown that microporous zeolites have a good catalytic effect on the copyrolysis process and improve the yield and quality of aromatics. Kim et al.,[29] Pouya et al.,[30] and Chi et al.[22] have found that mesoporous sieve catalysts also enhanced the yield and quality of liquid oil during biomass copyrolysis; they obtained high-quality liquid oil with high calorific value and low acidity. However, different catalysts exhibit different catalytic activities in the catalytic process due to their different acidities and pore sizes. Kim et al.[31] investigated the co-pyrolysis process of box-wood with plastic wastes in microporous HZSM-5 and mesoporous Al-MCM-41 catalytic conditions, and the two catalysts with different acidities and pore sizes could improve the yield of aromatics, with the microporous HZSM-5 showing higher activity. Kim et al.[32,33] studied the catalytic performance of different pore sizes and acidity catalysts for the preparation of high-quality liquid oil via biomass and have found that the catalytic performance of different catalysts for biomass is different. Shafaghat[34] and Kim[35] also found that catalyst pore size and acidity were important factors affecting biomass pyrolysis. However, most previous studies focused on the interaction of the acidity and pore size of catalysts, whereas the separate effects of acidity and pore size have been less studied.

In this study, four biomass-based catalysts with different pore sizes and basically the same acid content were used as research objects to investigate the influence of the pore size and active center of catalyst carrier on biomass pyrolysis. The liquid phase products were analyzed by Gas Chromatography-Mass Spectrometer (GC-MS), and the biomass-based catalysts were characterized by BET, TPD, XRD, FTIR and other detection methods. The optimum catalyst aperture for BTX preparation and optimal cycling performance were determined among the four catalysts. Among the biomass-based catalysts supported by the three metal active centers, the catalyst with better catalytic activity was found.

2. Materials and methods

2.1 *Experimental materials*

WNSs were purchased from Zhengzhou, Henan Province, China. PP was purchased from Shenhua Chemical Co., Ltd., Ningxia Shenhua Coal 1100 n. The WNSs were washed and dried at 105 °C for 24 h before experimental use. The WNSs and PP were crushed by using a shredder. WNS used in the experiment was less than 100 mesh. Similarly, during the experiment, PP was less than 30 mesh and it was dried at 80 °C for 24 h. The elemental and industrial analyses of WNS are shown in Table 1.

Table 1. Industrial analysis and elemental analysis of walnut shell

Samples	Elemental analysis (wt%, ad)					Industrial analysis (wt%, ad)			
	C	H	O[a]	N	S	M	A	V	FC
Walnut shell	49.936	5.856	43.962	0.203	0.043	6.213	1.861	81.234	10.692

Note: [a] indicates the use of differential subtraction; ad: air-dried basis. M: Moisture; A: Ash; V: Volatile; FC: Fixed-carbon

2.2 *Preparation of catalyst*

2.2.1 *Preparation of biomass coke*

Biomass coke was prepared in a tube furnace by weighing an appropriate amount of WNS powder (below 100 mesh). Argon gas was introduced into the tubular furnace and purged for 15 min. The temperature rose to 850 °C at a rate of 10 °C/min and biomass coke was obtained after 15 min thermolysis.

2.2.2 *Preparation of biomass-based catalysts*

A 2.5-g biomass coke was placed in a tube furnace and purged with argon for 15 min. The heating rate was 10 °C/min. Water vapor was supplied when the temperature increased to 850 °C. The steam activation time was 35, 40, 75, and 80 min. The realized biomass-based catalysts were named 1-F, 2-F, 3-F, and 4-F, respectively. The metal ions in the biomass-based catalyst were washed with 3 mol/L hydrochloric acid and then washed repeatedly with deionized water until the pH value was approximately 7. Afterward, the biomass-based catalysts were dried for later use. After 10 cycles, the biomass-based catalysts were named 1-X, 2-X, 3-X, and 4-X in turn.

2.2.3 *Preparation of loaded active center catalyst*

The catalyst was prepared by the traditional wet impregnation method. 0.2 g $Ni(NO_3)_2 \cdot 6H_2O$, $Zn(NO_3)_2 \cdot 6H_2O$, $Ce(NO_3)_3 \cdot 6H_2O$ were mixed with biomass-based catalyst 1-F in a mass ratio of 1:10, and the solvent was 20 mL anhydrous ethanol. The prepared solution was stirred at 40 °C for 10 h until the anhydrous ethanol volatilized, and dried in the oven at 100 °C for 12 h. The prepared catalysts were named Zn-1-F, Ni-1-F, and Ce-1-F; the reacted catalysts were named Zn-1-R, Ni-1-R, and Ce-1-R.

2.3 *Catalyst characterization*

The specific surface area and pore size distribution of the catalysts were characterized by KANTA AUTOSORB IQ automatic physical and chemical adsorption apparatus. The specific surface area was obtained by linear regression with the Brunauer Emmett Teller model, and the aperture distribution was calculated by using DFT (density functional theory) model. NH_3-TPD (temperature-programmed desorption) chemisorption was performed by using a multifunctional adsorption apparatus (Sincere TP-5080) to determine the acidity and acid amount of the biomass-based catalysts. The metallic-doped catalysts were characterized by using an X-ray diffractometer (XRD, D8 AdvanceA25) made by Brooke AG, Germany.

2.4 *Pyrolysis experiments*

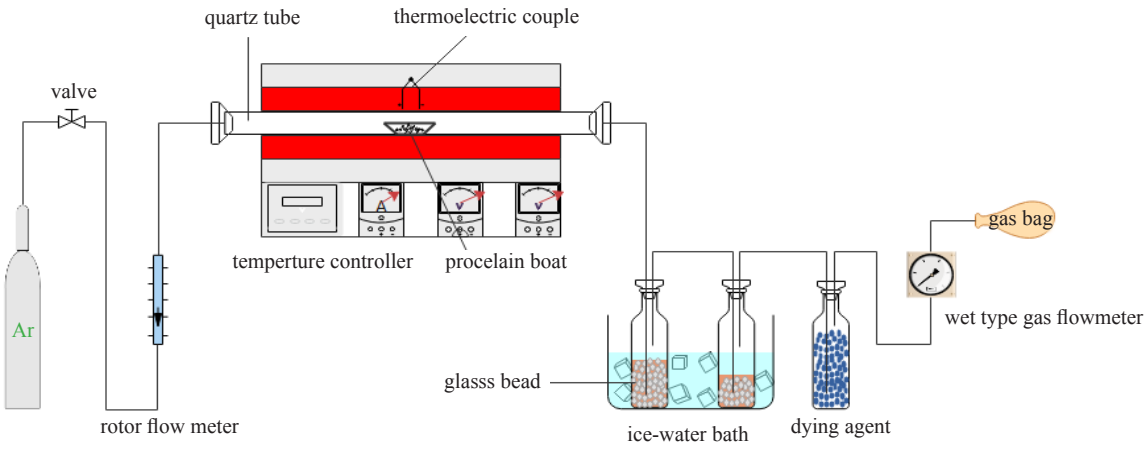

Figure 1. Pyrolysis experimental device diagram

The experimental device is shown in Figure 1. The amount of WNS, PP, and catalyst used in the experiment was 2 g. Before the experiment, argon was purged for 30 min with a gas flow of 200 mL/min and then the temperature was increased to 600 for 15 min. The liquid products were collected with isopropanol as absorbents. Each catalyst was subjected to 10 cyclic pyrolysis experiments, and the liquid products of the 1st, 2nd, 5th, and 10th cycles were collected and analyzed using GC-MS.

2.5 *External quantification of BTX*

The yields of BTX produced by a biomass-based catalyst and WNS/PP were determined through an external standard method. Standard solutions of different concentrations (0.1, 0.3, 0.5, 0.7, and 0.9 g/L) were prepared with single cyclic aromatic hydrocarbons and analyzed using GC-MS. A standard curve was established based on the concentration of monocyclic aromatic hydrocarbons (g/L) and the peak area of GC-MS, and the product BTX was quantified according to its standard curve. The calculation formula is as follows:

$$\frac{A_0}{C_0} = \frac{A_n}{C_n}$$

A_0: Peak area of mass spectra of standard monocyclic aromatic hydrocarbons;
C_0: The concentrations of the standard monocyclic aromatic hydrocarbons are known, mg/L;
A_n: Peak area of mass spectra of monocyclic aromatic hydrocarbons in liquid products;
C_n: Concentration of monocyclic aromatic hydrocarbons in liquid phase products, mg/L.

3. Results and discussion

3.1 *Effect of different pore size catalysts on the production of BTX from WNS/PP*

3.1.1 *Analysis of GC-MS results of pyrolysis liquid phase products with 10 catalyst cycles*

Table 2. GC-MS analysis of liquid products of walnut shell/polypropylene catalyzed by catalysts with different pore sizes

Catalyst type	Number of cycles/times	C_6H_6	C_7H_8	C_8H_{10}	Total BTX
1-F	1	-	8.10	4.84	12.94
	2	-	15.41	5.51	20.92
	5	-	9.35	0.48	9.83
	10	-	-	0.66	0.66
2-F	1	-	2.51	1.46	3.97
	2	-	-	3.40	3.40
	5	-	-	-	-
	10	-	-	0.83	0.83
3-F	1	-	2.93	1.40	4.33
	2	-	3.42	0.96	4.38
	5	-	-	2.14	2.14
	10	-	-	0.89	0.89
4-F	1	-	0.29	1.18	1.47
	2	-	-	3.20	3.20
	5	-	-	1.42	1.42
	10	-	-	0.15	0.15

Note: The values of products in the table indicate the percentage of peak area of mass spectrometry peaks

The experimental results are shown in Table 2. The relative BTX contents in the liquid-phase products differed significantly when the four catalysts were cycled the same number of times. The relative BTX contents in the liquid-phase products of the first, second, and fifth cycles were from 1-F > 3-F > 2-F > 4-F. After adding 1-F to WNS/PP, the relative BTX contents in the liquid-phase products were significantly higher than that of the remaining three catalysts, with the relative BTX contents in the first, second, and fifth cycles being 12.94, 20.92, and 9 area%, respectively. Nevertheless, the relative BTX contents of the other three catalysts in the first, second, and fifth cycles were not higher than 5 area%. The relative BTX content of the liquid-phase products was less than 1 area%, indicating that the catalyst activity was very low and deactivated after 10 cycles. In conclusion, the superior performance of catalyst 1-F in the WNS/PP process for the preparation of aromatics was observed.

3.1.2 *Effect of pore size distribution of the four catalysts on BTX production*

Figures 2(a), (b), (c), and (d) show the pore-size distribution of catalysts 1-F, 2-F, 3-F, and 4-F, respectively. In Figure 2(a), the pore sizes of 1-F were mainly concentrated around 0.55 and 1.2 nm, which is a primarily microporous structure. The pore size of 2-F was mainly distributed around 0.5 nm, but there was a large number of pore structures between 1 and 5 nm, so the structure of 2-F was between micropores and mesopores, (Figure 2(b)). As shown in Figure 2(c), the pore size of 3-F was mainly distributed around 3.7 nm, but there was also a small number of pores between 0.7 and 2 nm, which were mainly mesoporous structures. As shown in Figure 2(d), the 4-F was mainly mesoporous structure, and its pore size ranged from 0.5 to 7 nm and more at 3-7 nm. The pore size of 4-F was larger than that of 3-F. Therefore, the catalysts with four pore sizes were classified as microporous, micromesoporous, and mesoporous. The average pore size structure of the four catalysts was 1-F < 2-F < 3-F < 4-F.

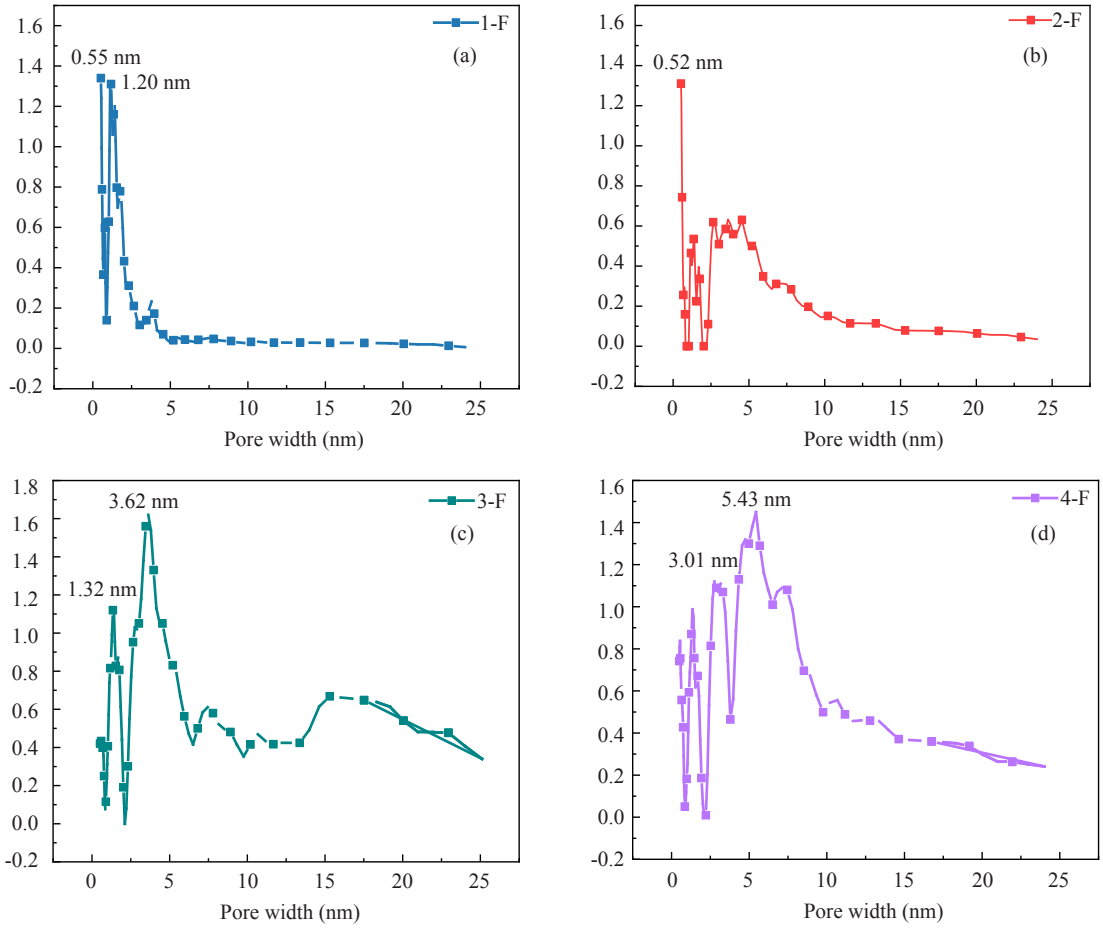

Figure 2. Pore size distribution of four fresh and reactive biomass bases

3.1.3 *The apparent morphology of four biomass-based catalysts*

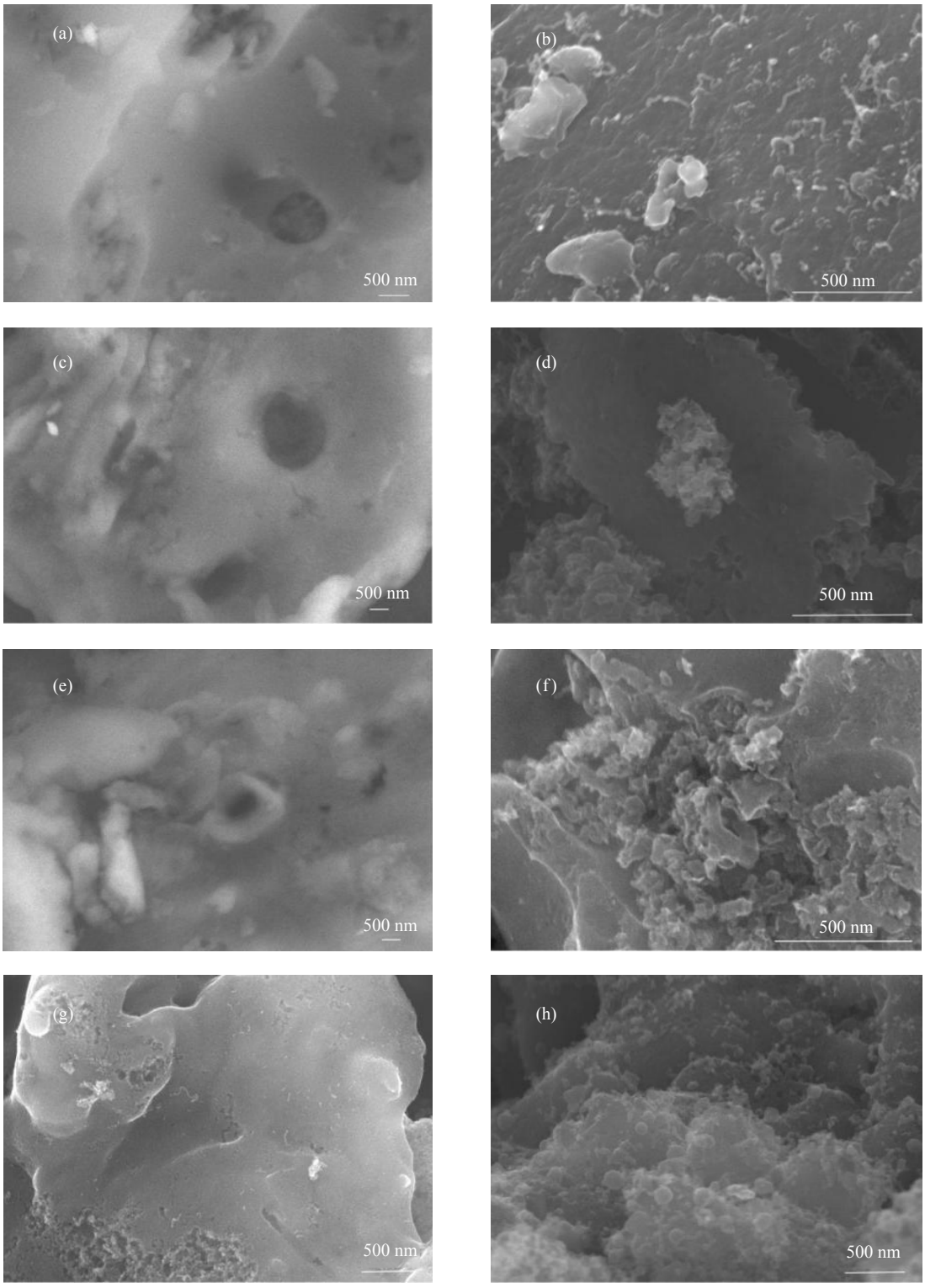

Figure 3. Fresh and 5-cycle morphology of 1-F (a, b), 2-F (c, d) , 3-F (e, f) and 4-F (g, h)

According to Figure 3, fresh biomass-based catalysts have a large number of pore structures. After five cycles of

pyrolysis experiments, a large number of coke deposits on the surface of biomass-based catalysts, resulting in pore blockage.

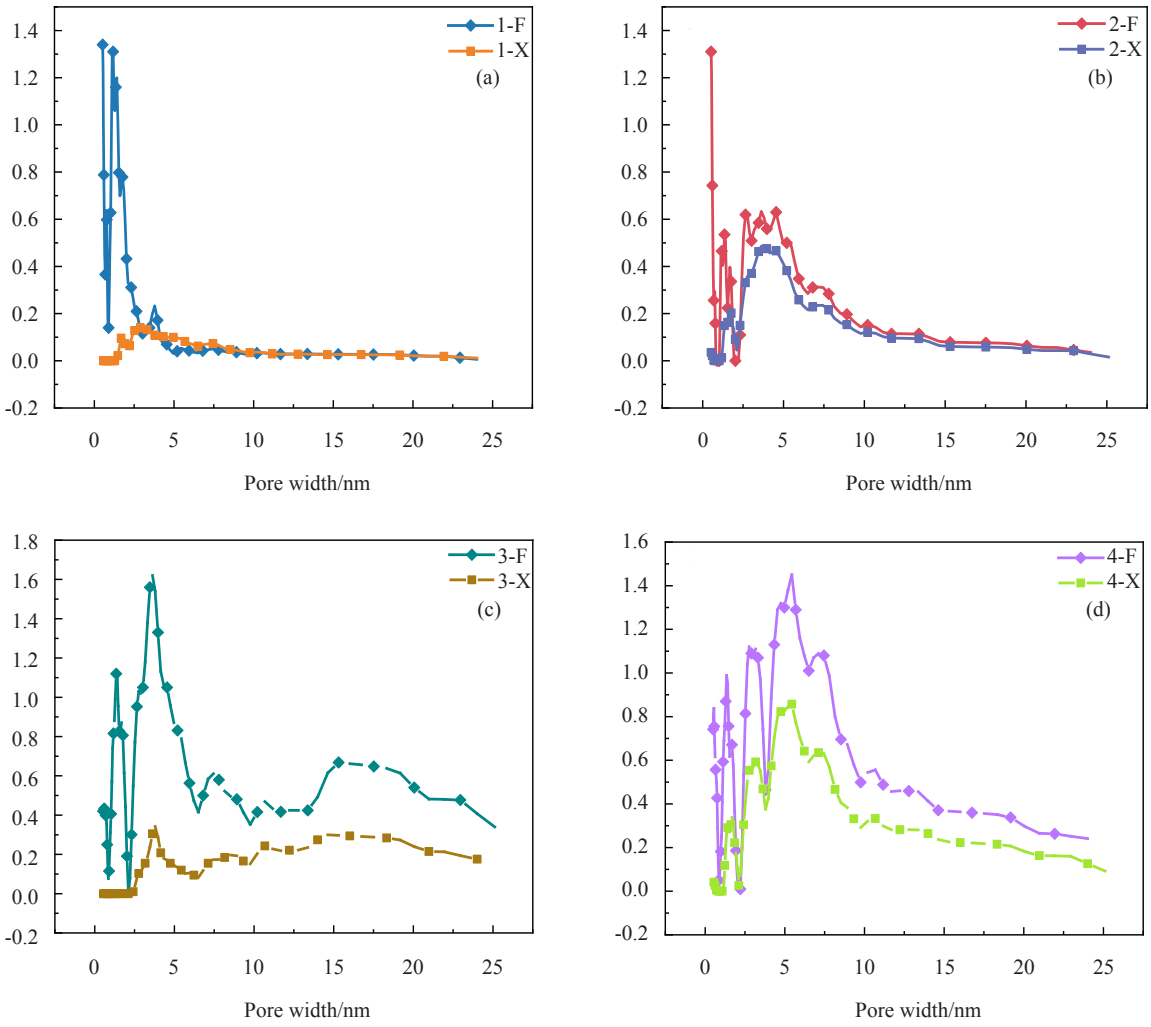

Figure 4. Comparison of pore size distribution of 4 fresh catalysts and 4 catalysts after 10 cycles

As shown in Figure 4, compared with the 4 fresh catalysts after 10 cycles, there was almost no microporous structure below 2 nm, but some mesoporous structures still existed. During the WNS/PP, as the pyrolytic volatiles entered inside the catalyst pore size, some organic macromolecules adhered to the pore channel, causing serious coking phenomenon and blockage of micropores. Therefore, the micropore structure was sharply reduced so that volatiles could not penetrate the pore channel and lacked selectivity for generating aromatic structures. The mesoporous structure of 3-7 nm was partially reduced, and the mesoporous structure was not coking due to its larger pore size. However, with the increase in the number of cycles, the continuous accumulation of biomass coke in the pore channel caused the blockage of the channel, so the mesoporous structure was also partially reduced. The results of the GC-MS analysis showed that when the catalyst was cycled twice, there were more microporous structures and BTX, but with the increase in the catalyst cycle time, the microporous structure was almost no longer found in the four catalysts. After 10 cycles, the relative BTX contents in the liquid-phase products were less than 1 area%, which indicated that the pore size of catalysts affected the relative BTX content. Meanwhile, from Figure 4(b), the 2-F catalyst pore size was concentrated at 0.52 nm, but the BTX content was far less than that of 1-F (d_p = 0.55-1.2 nm), indicating that a more concentrated and smaller

catalyst main pore size is probably rather unfavorable for the preparation of BTX in the biomass copyrolysis process.

From Table 3, the specific surface areas of the 1-F and 4-F catalysts were basically the same, but their BTX contents differed significantly. The specific surface areas of 2-F and 3-F catalysts had little difference, while their BTX contents differed significantly, indicating that the main factor affecting the BTX yield during the WNS/PP copyrolysis was the pore size, whereas the specific surface area of the catalysts had little effect. The pore structures present in the 4 fresh catalysts were basically mesoporous after 10 cycles, and the specific surface areas of the fresh catalysts were all less than those of the fresh catalysts.

Table 3. Physicochemical characterization of biomass-based catalysts

Catalyst type	1-F	1-X	2-F	2-X	3-F	3-X	4-F	4-X
$D_{poresize}$ (nm)	0.55-1.20	1.70-3.00	0.52, 1.50-5.00	3.70-4.50	3.00-4.00	3.00-4.00	3.00-7.00	3.00-7.00
S_{BET} (cm^2/g)	1384.59	80.01	862.07	254.09	729.01	74.60	1328.67	407.89
V_{total} (cm^3/g)	0.6715	0.0999	1.8110	0.3072	1.41	0.2889	1.284	0.5958

3.1.4 *Effect of acid content of biomass-based catalyst on catalytic co-pyrolysis of WNS-PP to BTX*

Table 4. Acid content of catalyst with four fresh biomass-based catalysts with different pore sizes

Sample	Sample quality	Sample peak area	Sample acid quantity	Total acid quantity (mmol/g)
1-F	0.0999	25078	0.000025078	2.350781902
1-X	0.0971	3921	0.000042252	0.435134378
2-F	0.0991	22878	0.000246527	2.487655200
2-X	0.0998	8867	0.000095548	0.957396755
3-F	0.0991	21996	0.000244780	2.479107256
3-X	0.0993	8559	0.000092229	0.928794344
4-F	0.0991	23021	0.000248068	2.503204405
4-X	0.0997	5235	0.000056411	0.565805691

Figure 5 shows the temperature-programmed adsorption curves of NH_3 for the four catalysts. As shown in Table 4, the acidities of the 4 fresh catalyst samples were higher than those of the 4 catalysts after 10 cycles, which illustrated that acid was consumed in the catalytic process and the acid on the catalyst surface is an essential factor affecting the distribution of biomass pyrolysis products. Meanwhile, the acidities of the biomasses based on the main pore size of 0.5 and 3-7 nm were basically the same, but according to the GC-MS results of the pyrolysis experiments, the biomass with

the main pore size of 0.55-1.2 nm was more conducive to BTX production.

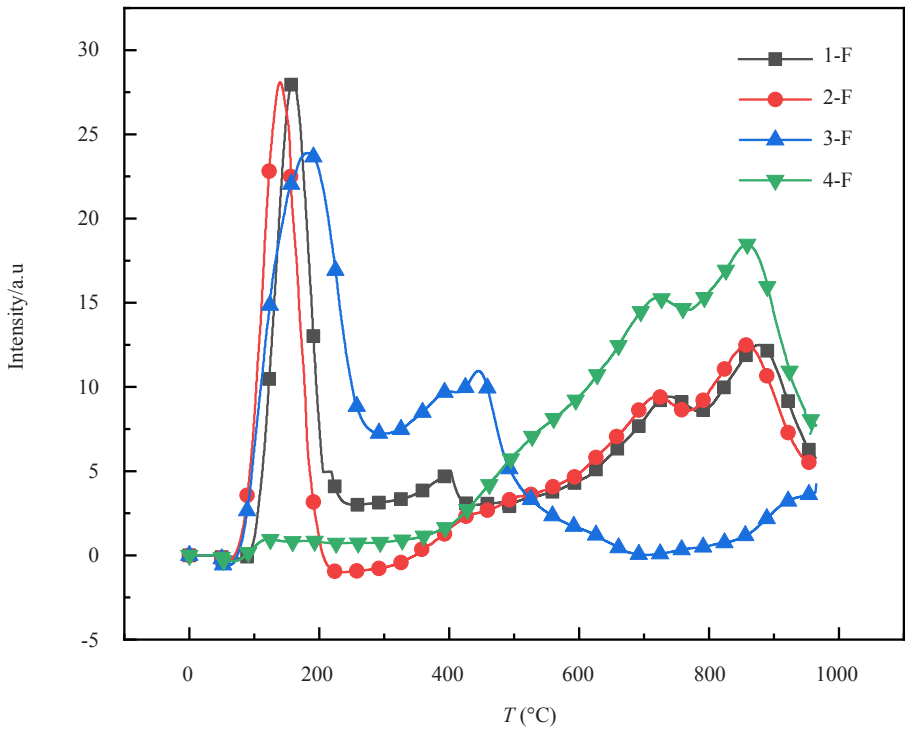

Figure 5. Temperature-programmed adsorption diagram of ammonia

3.1.5 *Changes in surface functional groups of biomass-based catalysts*

As shown in Figure 6, the most characteristic peaks of the four fresh biomass-based catalysts were between 3600~3300 cm^{-1} and 1700~600 cm^{-1}. The characteristic peak is about 3600~3300 cm^{-1}, and the absorption band is wide and blunt, mainly for phenolic and alcohol hydroxyl (OH-) stretching vibration; The peak of 3-F at 2900 cm^{-1} is mainly the stretching vibration of methyl (CH_3-). The characteristic peak at about 1580 cm^{-1} is weak, mainly the skeleton vibration of benzene ring, and the peak at about 1100 cm^{-1} is the bending vibration of the carbonyl group (-C = O). Biomass-based catalysts 1-F and 2-F showed a strong peak at about 1380 cm^{-1} with strong absorption strength, while 3-F and 4-F also showed a peak at about 1380 cm^{-1} with weak absorption strength. The characteristic peak at about 1380 cm^{-1} is mainly the bending vibration of CH_3-. The degree of absorption may be related to the pore size of the biomass-based catalyst.

As shown in Figure 7, after 10 cycles of pyrolysis experiments, the peak patterns of the infrared spectra of the four biomass-based catalysts were basically the same and the characteristic peaks appeared at about 3400 cm^{-1} and 1380 cm^{-1}, but the absorbency intensity was inconsistent. After 10 cycles of pyrolysis experiments, the absorbance of biomass-based 1-X, 2-X and 3-X was lower than that of fresh biomass-based catalysts 1-F, 2-F and 3-F, and the absorption intensity of characteristic peaks weakened. The results showed that a large amount of coke deposited on the surface of the biomass-based catalyst resulted in the decrease of the absorbance of the biomass-based catalyst. This is also consistent with the BET test results. With the increase of reaction times, the pore structure decreases and the reactivity decreases. However, the light absorption intensity of 4-F increases after the cyclic pyrolysis experiment, which may be due to the larger pore size of the biomass-based catalyst 4-F.

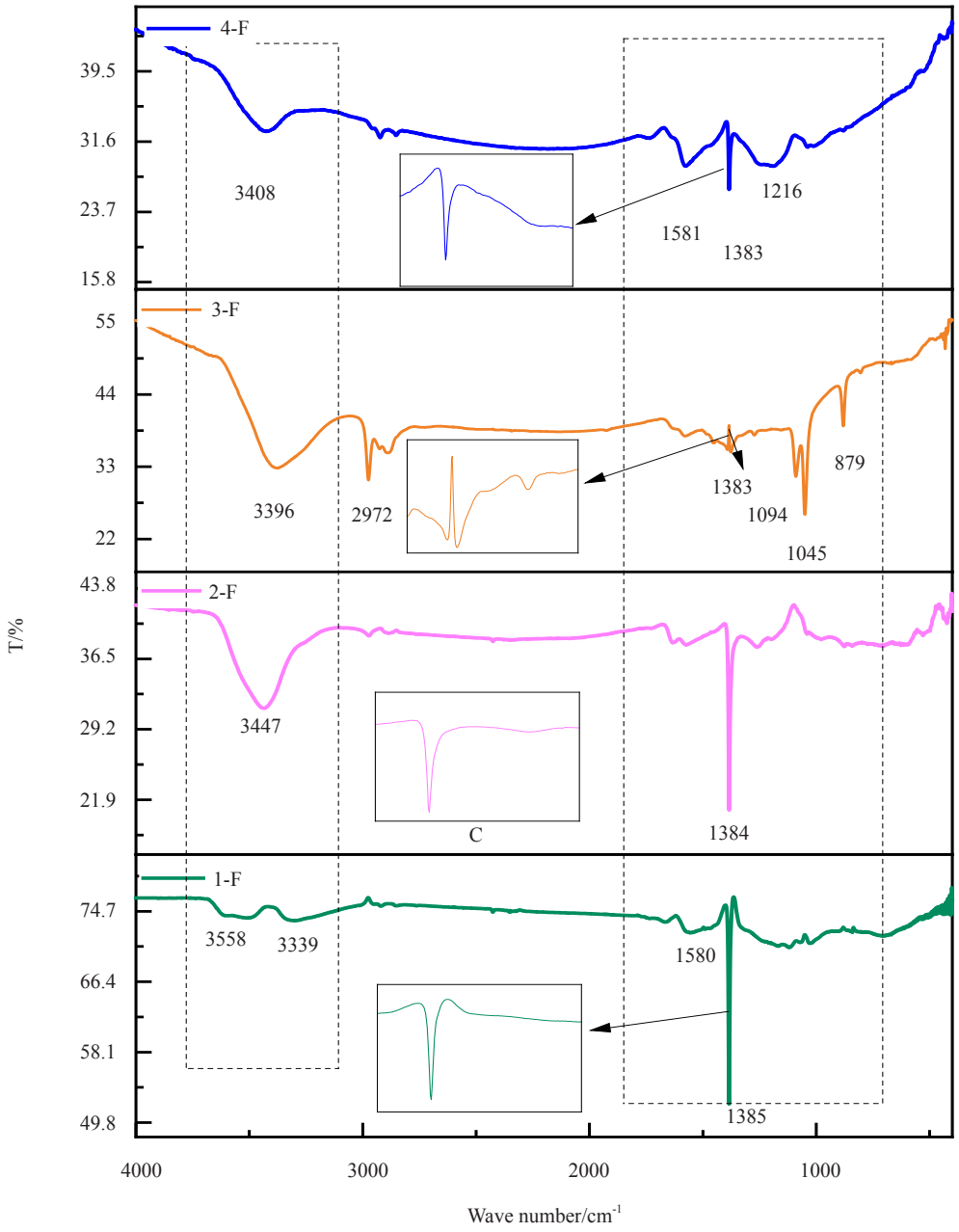

Figure 6. Infrared spectra of fresh biomass-based catalyst

3.2 *Effect of different metal components on the production of BTX from WNS/PP co-pyrolysis*

3.2.1 *XRD analysis*

As shown in Figure 8, the XRD patterns of fresh catalysts loaded with three elements showed no obvious peak position. Instead, the peak position was obvious after a reaction. The reason might be that during the metal-loading process, the metal is combined with the carbon in the biomass-based catalyst and unexposed on the surface, so there was no peak position in XRD. Meanwhile, after the reaction, the high temperature destroyed the carbon structure and made the metal exposed on the surface of the biomass-based catalyst, so the XRD pattern showed a peak pattern, especially for the Zn-loaded catalyst.

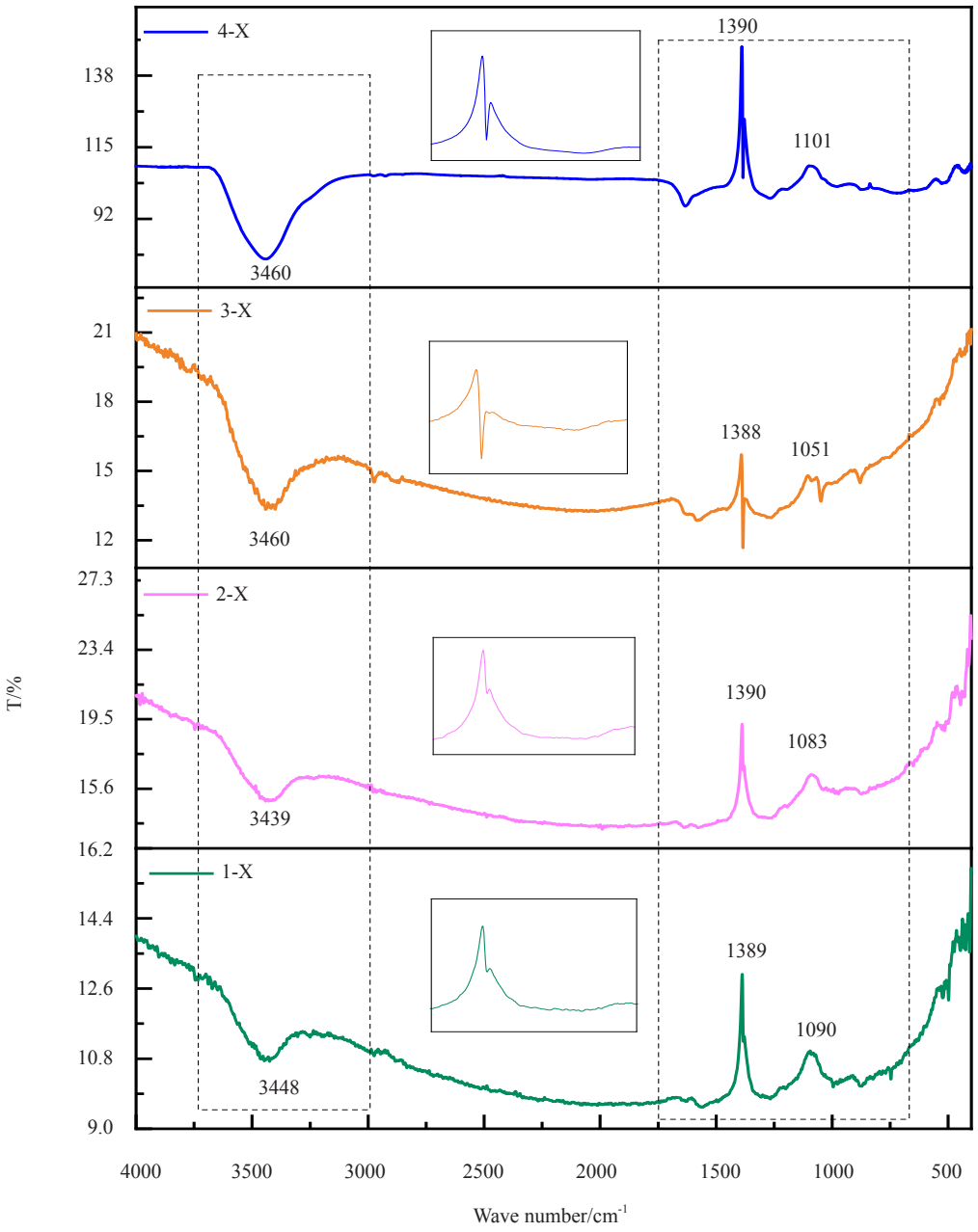

Figure 7. Biomass-based catalyst infrared spectra after reaction

3.2.2 *Analysis of liquid phase products after metal loading*

As shown in Table 5, after the 1-F catalyst, with a pore size of 0.55-1.2 nm, was loaded with Ce, Ni, and Zn, the relative aromatic hydrocarbon content produced by the copyrolysis of WNS/PP and catalyst increased compared with that of WNS/PP alone. Among them, the catalyst loaded with the transition metal, Zn, had the highest relative BTX content. The results demonstrated that the loading of metal-active centers on the catalysts could improve the reactivity of the catalysts and increase the relative BTX content in the liquid-phase products.

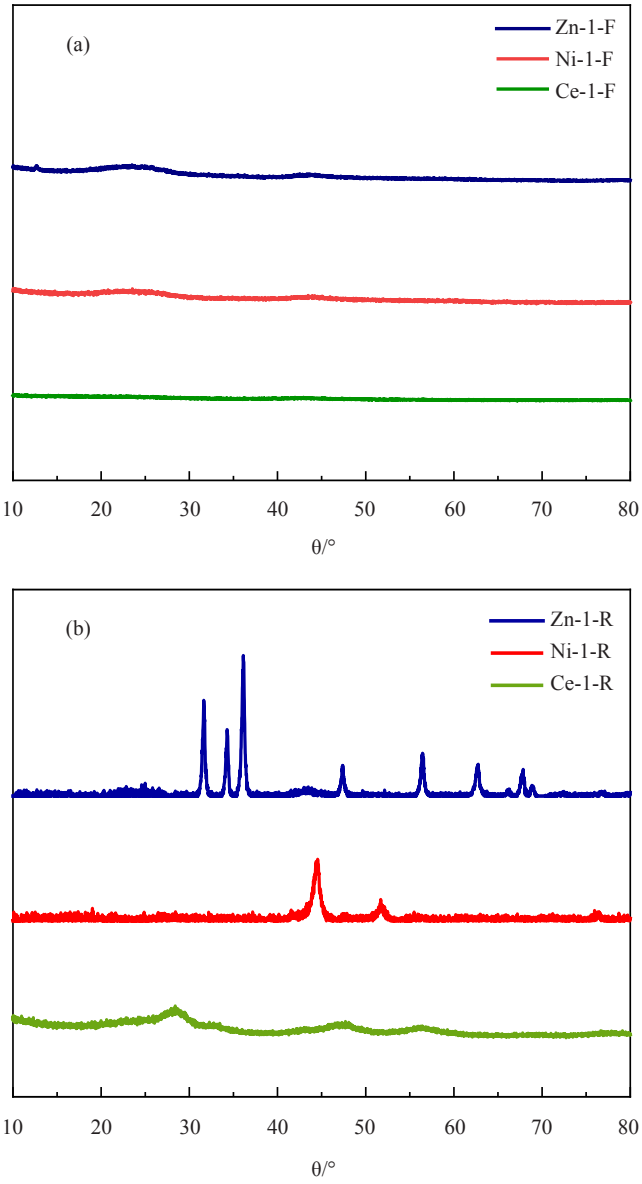

Figure 8. X-ray diffraction of catalyst; (a): X-ray diffraction patterns of three fresh metal catalysts; (b): X-ray diffraction of the three metal catalyst after reactions

Table 5. GC-MS analysis of 1-F catalyst after metal loading

	C_6H_6/area%	C_7H_8/area%	C_8H_{10}/area%	BTX/area%
Ce-1-F	2.30	15.00	1.49	18.79
Ni-1-F	2.80	22.50	2.01	27.31
Zn-1-F	3.10	30.10	6.39	39.59

3.2.3 *Analysis of pore size distribution and specific surface area of catalyst loaded active components*

As shown in Figures 9, 10, and 11, the pore sizes of both the fresh and reacted catalysts were dominated by micropores, ranging from 0.5 to 0.7 nm, after the 1-F catalyst was loaded with three different metal elements and there was no significant change in the pore structures and the number of micropores after one reaction. The pore sizes of the three metal-loaded catalysts were similar to those of the fresh catalysts, but the number of micropores reduced compared with that of the fresh catalysts. The reason for this is that some of the metal compounds penetrated the pore size and deposited on the pore surface during the loading process, resulting in smaller pore size, lower number of micropores, and fewer pores around 1 nm. Therefore, the main pore sizes of the metal-loaded catalysts were more concentrated in micropores below 1 nm, whereas the main pore size of the Ce-loaded catalyst was approximately 0.589 nm; that of the Ni- and Zn-loaded catalysts was approximately 0.64 nm. Further, the pore size of the Zn-loaded catalyst was the smallest among the three metal catalysts.

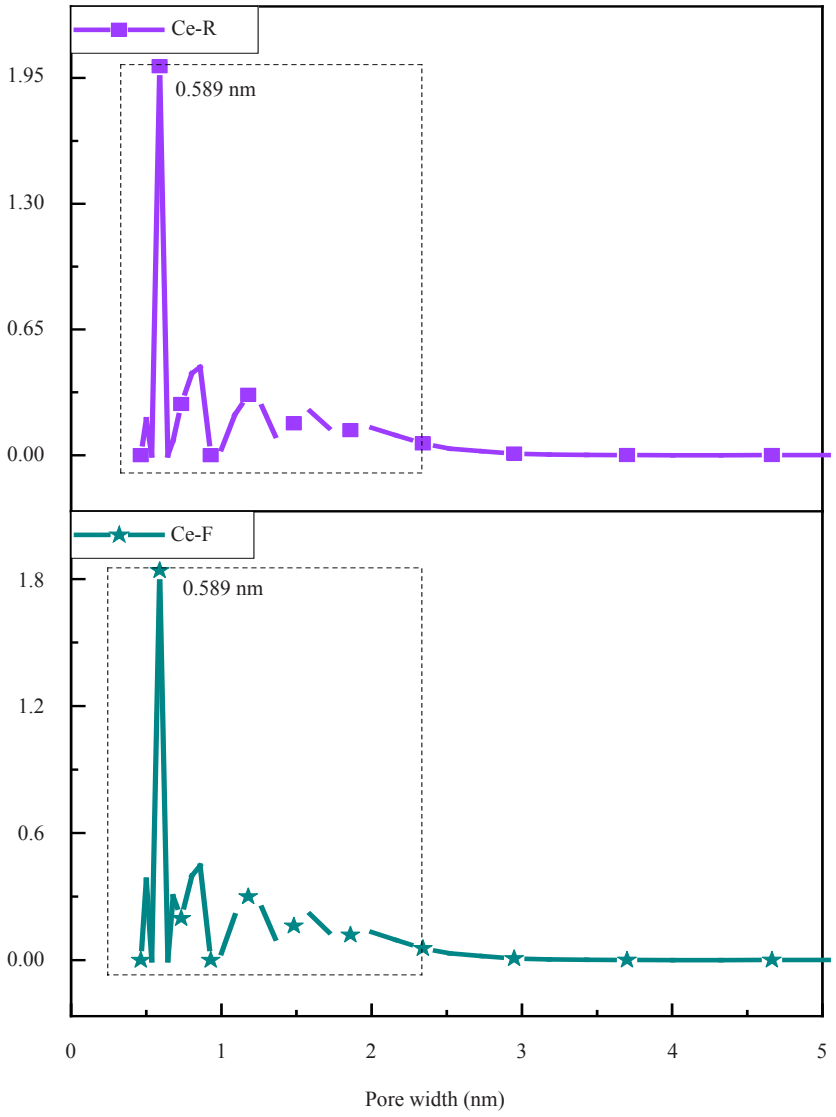

Figure 9. Pore size distribution of the Ce-1-F and Ce-1-R catalysts

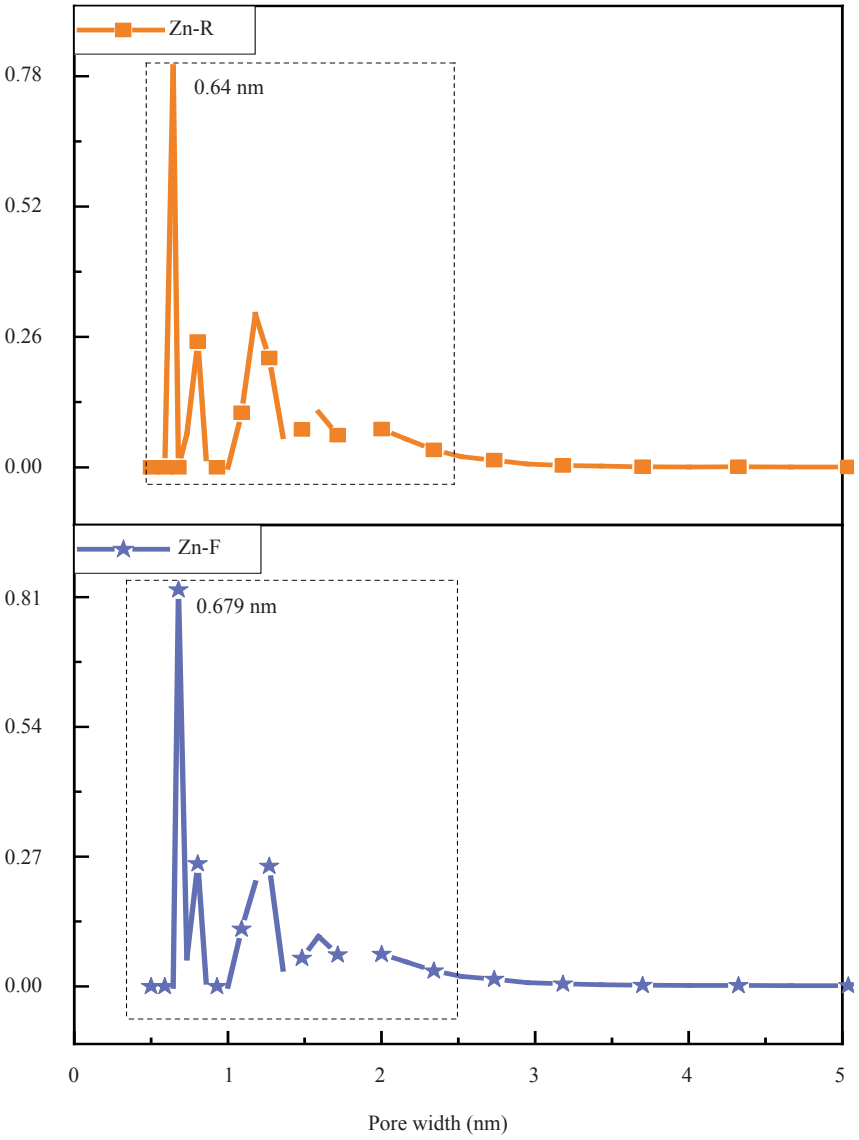

Figure 10. Pore size distribution of the Zn-1-F and Zn-1-R catalysts

Table 6. Physicochemical characterization of metal-loaded catalysts

	Ce-1-F	Ni-1-F	Zn-1-F
$D_{Pore\ size}$ (nm)	0.589	0.500–0.589	0.640
S_{BET} (cm^2/g)	944.375	1014.446	422.842

The pore sizes of the three metal-loaded catalysts were in the order of Zn-1-F > Ce-1-F > Ni-1-F, but their specific surface areas were in the order of Ni-1-F > Ce-1-F > Zn-1-F (Table 6). Combining the pore sizes and specific surface areas after metal loading with the analysis of the GC-MS results of the pyrolysis experiments in Table 5, Zn-1-F had the best catalytic effect during the pyrolysis process. The results suggested that it was the metal-active center that played a

crucial role in the preparation of aromatics by WNS/PP pyrolysis when the biomass base was loaded with active centers, which might also be related to the pore size and specific surface area.

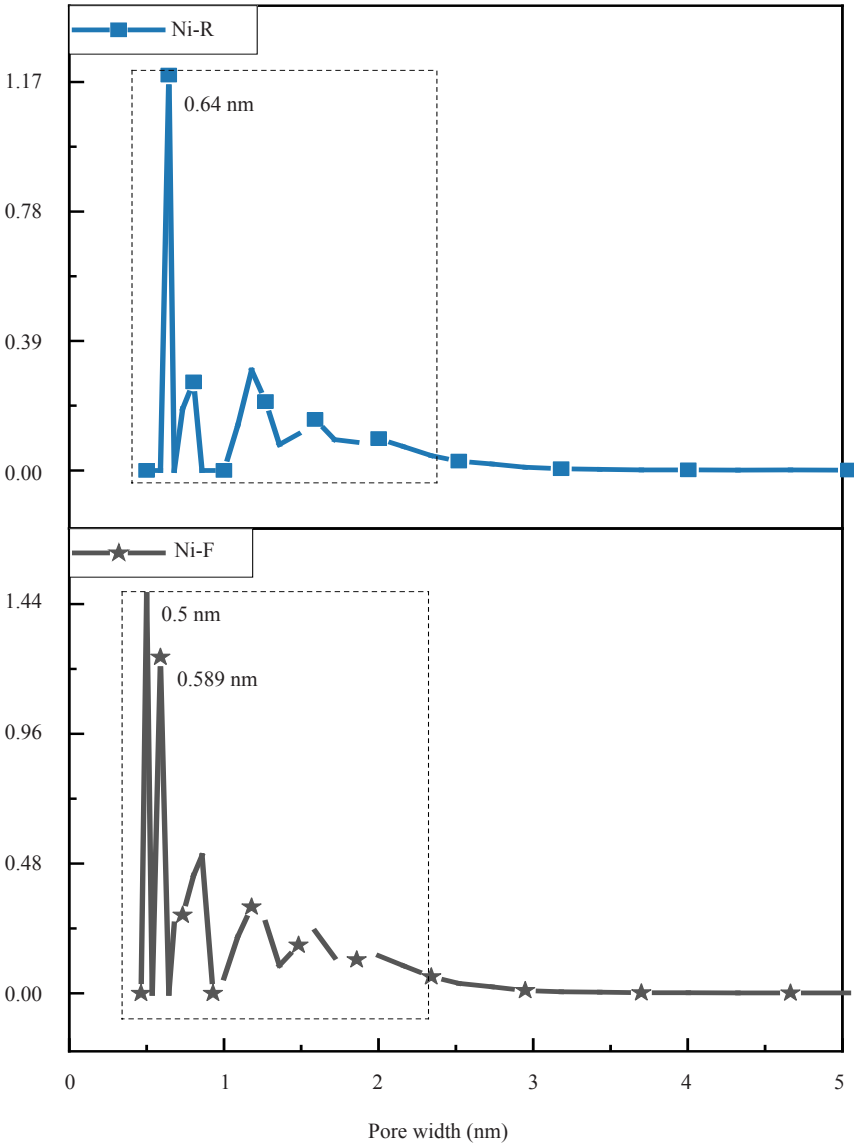

Figure 11. Pore size distribution of the Ni-1-F and Ni-1-R catalysts

3.3 *Quantitative analysis of BTX yield by external standard method*

From Table 7, in the WNS/PP copyrolysis process, the microporous catalyst with a pore size of 0.55-1.2 nm had the best effect on BTX production, and the BTX yield was 23-67 mg/(g_{raw}). The yield of the other three catalysts with large pore sizes was all below 20 mg/(g_{raw}). As shown in Table 8, in the WNS/PP copyrolysis process, the catalyst supported with Zn metal-active center had the best effect, and the BTX yield was as high as 111.13 mg/(g_{raw}). Compared with the catalyst without metal loading, the yield increased by 39.7%.

Table 7. Aromatic quantitative results for two cycles of catalyst support with different pore sizes

Biomass-based type	Number of cycle experiments	Peak area				External quantification (mg/L)	Recovery rate (mg/g)
		C_6H_6	C_7H_8	C_8H_{10}	Total aromatic peak area		
1-F	1.00	-	8694679.96	5685083.79	14379763.75	1178.22	23.56
	2.00	-	37185414.83	4076385.53	41261800.36	3380.81	67.62
2-F	1.00		0.00	3140886.11	3140886.11	257.35	5.15
	2.00	-	0.00	2397157.00	2397157.00	196.41	3.93
3-F	1.00	-	5438568.83	2595386.80	8033955.63	658.27	13.17
	2.00	-	5414039.67	1514844.62	6928884.29	567.72	11.35
4-F	1.00	-	91241.91	371144.88	462386.79	37.89	0.76
	2.00	-	-	1006556.28	1006556.28	82.47	1.65

Table 8. Aromatic quantitative results of active sites supported on the catalyst

Catalyst type	C_6H_6	C_7H_8	C_8H_{10}	Total aromatic peak area	External quantification (mg/L)	Recovery rate (mg/g)
Ce-1-F	4152931.76	27084337.55	2690377.53	33927646.84	2779.88	55.60
Ni-1-F	4128953.10	33179087.35	2963998.47	40272038.91	3299.72	65.99
Zn-1-F	5192248.74	51922487.35	10702732.07	67817468.16	5556.67	111.13

4. Conclusions

In this study, four kinds of catalysts with different pore sizes were used for cyclic pyrolysis experiments to select the most suitable catalyst pore size for BTX production, and three metal compounds were loaded on the catalyst with the optimum pore size for the BTX production to perform WNS/PP experiments. The following conclusions are obtained.

(1) The pore size is an essential factor affecting the BTX production from biomass, and the microporous structure with a pore size between 0.55 and 1.2 nm is more favorable for BTX production than the mesoporous structure with a pore size between 3 and 7 nm. The relative BTX content is between 9 and 20 area%, and the BTX yield is between 23 and 67 mg/(g_{raw}).

(2) Comparing the four kinds of catalyst support, the microporous catalyst 1-F has the best cycling performance and the relative BTX content is above 9 area% after five cycles.

(3) Three metal-active centers are added on the microporous catalysts with pore sizes between 0.55 and 1.2 nm for WNS/PP catalytic experiments. The results show that the Zn-loaded catalyst is the most conducive for BTX production, and the relative BTX content is 39.49 area% and the yield is 111.13 mg/(g_{raw}), which increases by 39.7%.

(4) The catalyst pore size and active center are the main factors affecting the WNS/PP.

Acknowledgement

This work was supported by the key research and development program of Ningxia province of China [2018BEE03009]; and the National Key Research and Development Program of China [2018YFB0605401]; the National Natural Science Foundation of China [21868025]; and Major Program of Key Research and Development Program of Ningxia Province of China [2018BCE01002].

Credit authorship contribution statement

Yanan Guo: Investigation, Methodology, Formal analysis, Writing-original draft, Writing-review & editing, Conceptualization;

Xin Pan: Writing-Reviewing and Editing;

Qingjiao Zhu: Methodology, Supervision;

Jingjing Ma: Writing-review & editing, Resources, Supervision, Validation;

Qingjie Guo: Writing-review & editing, Resources, Supervision, Validation.

Conflict of interest statement

We declare that we have no financial and personal relationships with other people or organizations that can inappropriately influence our work; there is no professional or other personal interest of any nature or kind in any product, service or company that could be construed as influencing the position presented in, or the review of, the manuscript entitled.

References

[1] Xue, J. J.; Zhuo, J. K.; Liu, M.; Chi, Y. C.; Zhang, D. H.; Yao, Q. *Energ. Fuel*. **2017,** *31*, 9576-9584.
[2] Wu, X. Y.; Wu, Y. L.; Wu, K. J.; Chen, Y.; Hu, H. S.; Yang, M. D. *Bioresource Technol*. **2015,** *192*, 522-528.
[3] Qin, L. Y.; Wu, Y.; Hou, Z. W.; Jiang, E. C. *Bioresource Technol*. **2020,** *313*, 123682.
[4] Akancha; Kumari, N.; Singh, R. K. *J. Energy Inst*. **2019,** *92*, 933-946.
[5] Chen, R. J.; Zhang, J. H.; Lun, L. Y.; Li, Q. H.; Zhang, Y. G. *Bioresource Technol*. **2019,** *292*: 121970.
[6] Nallar, M.; Wong, H. W. *Ind. Eng. Chem. Res*. **2019,** *58*, 10776-10784.
[7] Chen, L.; Wang, S. Z.; Meng, H. Y.; Wu, Z. Q.; Zhao, J. *Appl. Therm. Een*. **2017,** *111*, 834-846.
[8] Park, Y. K.; Lee, B.; Lee, H. W.; Watanabe, A.; Jae, J.; Tsang, Y. F.; Kim, Y. M. *Chem. Eng. J*. **2019,** *378*, 122151.
[9] Zhang, H. Y.; Nie, J. L.; Xiao, R.; Jin, B. S.; Dong, C. Q.; Xiao, G. M. *Energ. Fuel*. **2014,** *28*, 1940-1947.
[10] Paul, T.; Williams, Elizabeth, A.; Williams. *Energ. Fuel*. **1999,** *13*, 188-196.
[11] Predel, M.; Kaminsky, W. *Polym. Degrad. Stabll*. **2000,** *7*, 373-385.
[12] Jin, Z. J.; Yin, L. J.; Chen, D. Z.; Jia, Y. J.; Yuan, J.; Hu, Y. Y. *Chinese J. Chen. Eng*. **2018,** *26*, 180-188.
[13] Ozsin, G.; Putun, A. E. *Korean J. Chem. Eng*. **2018,** *35*, 428-437.
[14] Sajdak, M. J. *Anal. Appl. Pyrol.* **2017,** *124*, 415-425.
[15] Johansson, A. C.; Sandstrom, L.; Ohrman, O. G. W.; Jilvero, H. *J. Anal. Appl. Pyrol*. **2018,** *134*, 102-113.
[16] Dewangan, A.; Pradhan, D.; Singh, R. K. *Fuel*. **2016,** *185*, 508-516.
[17] Burra, K. G.; Gupta, A. K. *Appl. Energ*. **2018,** *220*, 408-418.
[18] Hua, D. R.; Wu, Y. L.; Chen, Y.; Li, J.; Yang, M. D.; Lu, X. N. *Catalysts*. **2015,** *5*, 2085-2097.
[19] Larsen, M. B.; Schultz, L.; Glarborg, P.; Skaarup-Jensen, L.; Dam-Johansen, K.; Frandsen, F.; Henriksen, U. *Fuel*. **2006,** *85*, 1335-1345.
[20] Li, K. X.; Lei, J. X.; Yuan, G. A.; Weerachanchai, P.; Wang, J. Y.; Zhao, J.; Yang, Y. H. *Chem. Eng. J*. **2017,** *317*, 800-809.
[21] Chattopadhyay, J.; Pathak, T. S.; Srivastava, R.; Singh, A. C. *Energy*. **2016,** *103*, 513-521.
[22] Chi, Y. C.; Xue, J. J.; Zhuo, J. K.; Zhang, D. H.; Liu, M.; Yao, Q. *Sci. Total. Environ*. **2018,** *633*, 1105-1113.

[23] Lin, X. N.; Zhang, Z. J.; Tan, S.; Wang, F. Q.; Song, Y. M.; Wang, Q. W.; Pittman, C. U. *Energ. Convers. Manage*. **2017,** *141*, 206-215.
[24] Hong, Y.; Lee, Y.; Rezaei, P. S.; Kim, B. S.; Jeon, J. K.; Jae, J.; Jung, S. C.; Kim, S. C.; Park, Y. K. *Catal. Today*. **2017,** *293*, 151-158.
[25] Qi, P. Y.; Chang, G. Z.; Wang, H. C.; Zhang, X. L.; Guo, Q. J. *J. Anal. Appl. Pyrol*. **2018,** *136*, 178-185.
[26] Lee, H. W.; Kim, Y. M.; Jae, J.; Jeon, J. K.; Jung, S. C.; Kim, S. C.; Park, Y. K. *Energ. Convers. Manage*. **2016,** *129*, 81-88.
[27] Lin, X. N.; Zhang, Z. J.; Wang, Q. W. *Energy*. **2019,** *189*, 116174.
[28] Zhao, Y. F.; Wang, Y. P.; Duan, D.; Ruan, R.; Fan, L. L.; Zhou, Y.; Dai, L. L.; Lv, J. Q.; Liu, Y. H. *Bioresource Technol*. **2018,** *249*, 69-75.
[29] Kim, H.; Choi, S. J.; Kim, J. M.; Jeon, J. K.; Park, S. H.; Jung, S. C.; Kim, S. C.; Park, Y. K. *Mater. Res. Bull*. **2016,** *82*, 61-66.
[30] Rezaei, P. S.; Oh, D.; Hong, Y.; Kim, Y. M.; Jae, J.; Jung, S. C.; Jeon, J. K.; Park, Y. K. *Energ. Convers. Manage*. **2017,** *151*, 116-122.
[31] Kim, Y. M.; Jae, J.; Kim, B. S.; Hong, Y.; Jung, S. C.; Park, Y. K. *Energ. Convers. Manage*. **2017,** *149*, 966-973.
[32] Kim, Y. M.; Jeong, J.; Ryu, S.; Lee, H. W.; Jung, J. S.; Siddiqui, M. Z.; Jung, S. C.; Jeon, J. K.; Jae, J.; Park, Y. K. *Energ. Convers. Manage*. **2019,** *195*, 727-737.
[33] Kim, Y. M.; Lee, H. W.; Choi, S. J.; Jeon, J. K.; Park, S. H.; Jung, S. C.; Kim, S. C.; Park, Y. K. *Int. J. Hydrogen Energ*. **2017,** *42*, 18434-18441.
[34] Shafaghat, H.; Lee, H. W.; Tsang, Y. F.; Oh, D.; Jae, J.; Jung, S-C.; Ko, C. H.; Lam, S. S.; Park, Y. K. *Chem. Eng. J*. **2019,** *366*, 330-338.
[35] Park, Y. K,; Lee, W. L,; Kim, Y. M. *J. Anal. Appl. Pyrol*. **2018,** *135*, 390-396.